Highlighting research from the Soft Matter, Rheology and Technology (SMaRT) and the Surface and Interface Engineered Materials (SIEM) groups of Profs. Christian Clasen and Jan Fransaer at KU Leuven, Belgium.

Sideways propelled bimetallic rods at the water/oil interface

Bimetallic Janus rods, dispersed at an interface between aqueous hydrogen peroxide solution and oil, show a significant enhancement of sideways self-propulsion motility in comparison to that observed near a solid wall.

Image credit: Gábor Szabó

As featured in:

See Christian Clasen *et al.*, *Soft Matter*, 2023, **19**, 6896.

ROYAL SOCIETY OF CHEMISTRY

rsc.li/soft-matter-journal

Registered charity number: 207890

Soft Matter

PAPER

View Article Online
View Journal | View Issue

Cite this: *Soft Matter*, 2023, **19**, 6896

Sideways propelled bimetallic rods at the water/oil interface†

Alina Arslanova, [a] Ine Matthé,[a] Olivier Deschaume, [b] Carmen Bartic, [b] Wouter Monnens, [c] Erwin Konrad Reichel, [d] Naveen Reddy, [ef] Jan Fransaer[c] and Christian Clasen *[a]

The motion of self-propelling microswimmers is significantly affected by confinement, which can enhance or reduce their mobility and also steer the direction of their propulsion. While their interactions with solid boundaries have already received considerable attention, many aspects of the influence of liquid–liquid interfaces (LLI) on active particle propulsion still remain unexplored. In this work, we studied the adsorption and motion of bimetallic Janus sideways propelled rods dispersed at the interface between an aqueous solution of hydrogen peroxide and oil. The wetting properties of the bimetallic rods result in a wide distribution of their velocities at the LLI. While a fraction of rods remain immotile, we note a significant enhancement of motility for the rest of the particles with velocities of up to 8 times higher in comparison to those observed near a solid wall. Liquid–liquid interfaces, therefore, can provide a new way to regulate the propulsion of bimetallic particles.

Received 8th April 2023,
Accepted 7th August 2023

DOI: 10.1039/d3sm00466j

rsc.li/soft-matter-journal

1. Introduction

The interest in self-propelled Janus particles is on the rise due to their promising applications in the manipulation of microscopic matter,[1–5] sensing[6] and drug delivery.[7,8] They typically consist of two surfaces with varying (electro-)chemical properties, which allows them to generate a gradient of chemical species along a Janus boundary and induce a fluid flow.[9–11]

Confinement has a large influence on the propulsion of Janus particles and can be used to drive their motion[12–14] as well as to modify their hydrodynamics[15,16] and the distribution of chemical species.[16,17] Propulsion near a bottom solid wall has received the most attention so far, since many chemically propelled Janus particles have metallic surfaces and thus sediment in aqueous solutions.[9] Compared to the motion near a solid boundary, the propulsion near and at liquid–fluid interfaces is less studied, especially for catalytic Janus particles moving due to the chemical decomposition of a fuel. For example, an interface-induced phoresis,[18,19] which involves a motion of a particle due to a symmetry breaking of the concentration of reagents or products at an interface, was predicted but never proven experimentally.

Liquid–fluid interfaces also allow the Janus particles to be irreversibly trapped and confine their motion in 2D. The number of studies on the adsorption and propulsion of active particles at liquid–fluid interfaces has significantly increased in recent years.[20,21] However, the current literature on the adsorption of Janus particles at liquid–fluid interfaces is, to a great extent, focused on polar/apolar Janus particles,[22,23] including studies of the influence of different shapes on their equilibrium orientation.[24–27] When Janus particles have two surfaces with a large contrast in wettability, each surface tends to stay in the phase with which it has the most affinity. A typical example is a Janus Pt/SiO_2 sphere, where the silica part is completely immersed in the water phase due to its hydrophilicity, while Pt is located in the *n*-decane phase.[28] This leads to the Janus boundary assuming a horizontal position along the liquid–liquid interface and, therefore, no propulsion. However, when the top and bottom phases of the LLI are swapped by flipping a specially designed microscopic cell so that the top phase is an aqueous hydrogen peroxide solution instead of a commonly lighter oil, the Janus particle initially dispersed in the hydrogen peroxide phase is not trapped at the LLI but propels slightly above it. A similar observation was made for the propulsion of Janus particles in the presence of oil droplets engineered by microfluidics.[29] Moreover, the experimentally observed contact angle and orientation of Janus colloids also greatly depend on

[a] *Department of Chemical Engineering, KU Leuven, 3001 Leuven, Belgium. E-mail: christian.clasen@kuleuven.be; Tel: +32 16 32 23 54*
[b] *Department of Physics, KU Leuven, 3001 Leuven, Belgium*
[c] *Department of Materials Engineering, KU Leuven, 3001 Leuven, Belgium*
[d] *Institute for Microelectronics and Microsensors, Johannes Kepler University, Altenberger Strasse 69, 4040 Linz, Austria*
[e] *Faculty of Engineering Technology, University of Hasselt, Martelarenlaan 42, 3500 Hasselt, Belgium*
[f] *IMO-IMOMEC, Wetenschapspark 1, 3590 Diepenbeek, Belgium*

† Electronic supplementary information (ESI) available. See DOI: https://doi.org/10.1039/d3sm00466j

their surface roughness (besides their surface chemistry), which leads to an observed pinning of the three-phase contact line in non-equilibrium positions and a variety of orientations.[30]

Studies on the propulsion of self-diffusiophoretic and self-electrophoretic Janus particles at the liquid–fluid interface are very limited, with only a few examples of propelling systems so far. Self-propulsion at air–water interfaces is typically characterized by large velocities, which surpass the velocity of Janus particles near a solid wall.[31,32] For example, a carbon fiber functionalized with glucose oxidase and bilirubin oxidase propels with velocities between 10^{-3} and 10^{-2} m s^{-1} at the interface between air and an aqueous D-glucose solution, which is related to the small viscous drag at the air–water interface as well as to large electric currents generated by the enzymatic reactions.[31] A two-fold increase in velocity compared to the propulsion in the bulk was also observed for Pt/SiO_2 spheres at the air–water interface.[32] Surprisingly, the more a Janus particle is immersed in the aqueous phase the faster it moves, which is a consequence of the random thermal fluctuations of the contact line between the particle and the air–water interface, leading to additional forces exerted on the particle.[33,34]

An opposite trend was shown by Dietrich *et al.*[30] for Pt/PS self-diffusiophoretic spheres propelling at the interface between hexadecane and an aqueous solution of hydrogen peroxide. The velocities of these Janus particles were smaller than the velocities of the same particles propelling near a solid wall because of the larger viscosity of hexadecane. The dependence of the self-diffusiophoretic velocity of Janus particles near a fluid–fluid interface on the viscosity ratio between the two fluids was also described theoretically by several groups.[35–37] In particular, a non-zero viscosity difference leads to the emergence of a torque and particle rotation around the axis parallel to the LLI.[37] At diminishing viscosity differences, rotational and translational velocity are reduced to their respective components in the bulk. However, it should be noted that these calculations are made with the assumption that both reactants and products can freely diffuse in both phases, which does not hold for the oil component.[37] Pt/Au nanorods propelling parallel to their long axis at the water/*n*-decane interface were also studied experimentally,[38] with more focus, however, on assessing the possibility of using them for the precise measurement of the surface shear viscosities by varying the concentration of surfactants dispersed in the aqueous phase.

A mechanism of Janus particle propulsion at the LLI was suggested for self-diffusiophoretic Pt/PS spheres by Dietrich *et al.*[30] According to their findings, the orientation of the platinum and polystyrene sides of the particle at the LLI dictates the strength of the interfacial chemical gradient, leading to a bimodal distribution of particle velocities. In particular, the more the catalytic side is submersed in the hydrogen peroxide phase, the less steep the gradient created along the LLI, resulting in smaller particle velocities.

The current study aims to expand the description of Janus particles at the LLI between an aqueous solution of hydrogen peroxide and oil beyond spherical geometries. We consider sideways propelled Pt/Au Janus particles, which, in contrast with previously studied systems, move by self-electrophoresis. This geometry can be beneficial for a range of applications where a larger active surface area is needed, in particular, for collection and transport of microscopic cargo.[39–42]

2. Materials and methods

2.1 Fabrication of sideways propelled Janus rods

The fabrication of sideways propelled Janus rods was adapted from previous publications.[40,41] A monolayer of aligned 3 μm diameter polystyrene fibers was produced by electrospinning a 25 wt% solution of polystyrene (PS, M_w = 280 kg mol^{-1}, Sigma Aldrich BVBA) in *N*,*N*-dimethylformamide (DMF, 99.8%, Acros Organics NV); parameters of electrospinning: voltage 22 kV, flow rate 0.2 mL h^{-1}, needle diameter 0.61 mm, temperature 34 °C, relative humidity 25 RH, distance between the needle and collector 13.5 cm. The alignment of fibers was achieved by using rectangular parallel electrodes[41,43] or a rotating drum collector (speed 1000–2000 rpm) coupled with a translating unit[44] (MTI, MSK-ESDC-3000).

The monolayer of PS fibers was sputter-coated (Quorum, Q150TS) with ~20 nm thick Pt/Pd and Au/Pd layers on opposite sides of the monolayer respectively, resulting in long Janus fibers. For simplicity these coatings will be referred to as Pt and Au coatings in this paper. For the preparation of the Janus rods, the Janus fibers were dispersed in liquid medium and cut into smaller rods of 10–100 μm length by ultrasonication using an ultrasonic probe (Hielscher UP400S, the total power 450 W) for 1.5 min. For the preparation of Janus rods for the measurements of a its velocity in 5 wt% H_2O_2 near a solid–liquid interface at the bottom of a microscopy cell, also referred to here as a solid wall, the fibres are dispersed in water. The separation distance between the rod and the solid wall is approximately 550 nm.[39] For liquid–liquid interface (LLI) experiments, the Janus fibers were dispersed in isopropanol (IPA) : water (2 : 3) solution prior to ultrasonication. Ultrasonication results in rods with a broad length distribution and bent rods.

2.2 Self-propulsion at the liquid–liquid interface

Before LLI experiments, *n*-decane (99+% pure, Acros Organics) was purified 3 times through a column of aluminum oxide (for chromatography, Brockmann 1, 40–300 μm, 60 Å, ACROS organics, neutral) to remove polar amphiphilic organic contaminants.

The sideways self-propulsion of Pt/Au rods at the LLI between an aqueous solution of hydrogen peroxide (5 wt%) and *n*-decane was captured with an inverted optical microscope (Olympus, IX71) with a 10× objective. The videos were then analyzed with a custom-written Python code to determine the particles trajectories and velocities.‡ The rod velocities were extracted from their displacement *via* image processing from

‡ The Python code for the tracking of the rods motion: **https://github.com/ReknowIndra/rod-track**.

the movies and averaged over the multiple consecutively captured frames. Decomposition of hydrogen peroxide gives rise to an additional displacement of particles in the microscopy cell due to convection, which was determined from the apparent motion of immobile particles and subtracted from the displacement of self-propelled rods.

2.3 Gel-trapping technique

The gel-trapping technique (GTT) was adapted from the procedure developed by Paunov and Cayre[45] and is used to measure the contact angle of the Janus rods at the oil/water interface by atomic force microscopy (AFM). In this procedure, 2 wt% of Phytagel (Sigma Aldrich) in MilliQ water is solubilized for 1 h at 80 °C. It was then added to a Petri dish and covered by purified *n*-decane. Janus rods were dispersed at the interface using a spreading solution of 2 : 3 IPA : water. The gel was further cooled to room temperature, after which the top layer of *n*-decane was removed. PDMS (Sylgard-184 Silicone Elastomer kit, initiator : elastomer 1 : 5, Sigma Aldrich) was cast on top of the gelled layer containing the particles. After the PDMS solidifies, the gelled layer was removed, revealing the particles trapped in the PDMS layer.

2.4 Contact angle measurements

Contact angles of bare and coated PS plates immersed in *n*-decane are measured with a sessile drop on a Theta Lite optical tensiometer (Biolin Scientific). For this, polystyrene plates are sputter-coated with Pt and Au using the same parameters and thickness as for the LLI experiments.

2.5 Atomic force microscopy (AFM)

An Agilent 5500 AFM with MAC III controller was used with NCHR probes (spring constant 42 N m^{-1}, resonance frequency 320 kHz, tip radius of curvature <8 nm) for the morphological imaging of the rods embedded in PDMS in intermittent contact (AAC) mode. The AFM images were leveled, line-corrected and measured (height profiles) using Gwyddion, a free and open-source SPM (scanning probe microscopy) data visualization and analysis software.[46]

2.6 Scanning electron microscopy (SEM) and energy-dispersive X-ray spectroscopy (EDX)

The morphology of the rods was analyzed using scanning electron microscopy (SEM) on a FEI Nova 600 Nanolab Nano-SEM. Energy-dispersive X-ray spectroscopy was used for elemental analysis (EDX; Octane elite super silicon drift detector, Ametek EDAX). An acceleration voltage of 10 keV was applied for all measurements.

3. Results and discussion

The sideways self-propulsion of Janus Pt/Au rods is studied at the interface between a 5 wt% aqueous solution of hydrogen peroxide and *n*-decane. To ensure a flat interface, the cell for microscopy measurements is designed with two wells of different diameter (Fig. 1) in order to pin the LLI at the edge.[28,30] Moreover, the diameter of the cell is designed to be significantly larger than the capillary length $\lambda_c = 4$ mm:

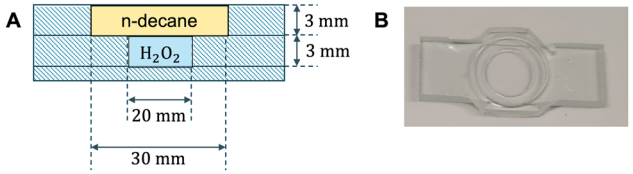

Fig. 1 The microscopy cell for LLI experiments. The cell consists of two wells of different diameters, which allows us to pin the interface between an aqueous solution of hydrogen peroxide and *n*-decane and obtain a flat interface. (A) The schematic showing dimensions of the cell; (B) the actual microscopic cell.

$$\lambda_c = \sqrt{\frac{\gamma_{w,d}}{\Delta\rho g}}, \quad (1)$$

where $\gamma_{w,d} = 53.2$ mN m^{-1} is the interfacial surface tension of the *n*-decane/water interface,[47] $\Delta\rho$ is the difference between the densities of two phases, and g is the gravitational acceleration constant [9.81 m s^{-2}].

The cell is sealed with a cover glass to reduce convection, which is, however, still present to a limited degree due to hydrogen peroxide decomposition and production of oxygen bubbles. These oxygen bubbles are trapped at the LLI due to capillary forces that counteract the buoyancy force and prevent them from crossing the LLI.[48]

Fig. 2 shows the typical motion of a Janus rod at the LLI (additionally, see Movie M1 in the ESI†).

The velocities of the sideways propelled Janus rods at the LLI shown in Fig. 3 are larger than their velocity of 1.82 ± 0.18 μm s^{-1} near a solid wall due to the smaller drag at the LLI. Note that the absolute viscosity of *n*-decane at room temperature $\eta_d = 0.84$ mPa s is close to that of water $\eta_w = 0.89$ mPa s,[49] which explains the apparent discrepancy of this result to the dynamics of Pt/PS spheres studied at the water/hexadecane interface.[30] Since the viscosity of hexadecane $\eta_h = 3.06$ mPa s is three times larger than that of water,[49] particles at the water/hexadecane interface experience an increased viscous drag, resulting in a lower velocity than that observed near the wall. As shown in Fig. 3A, the velocity of the Janus rods does not depend on the rod length, which is in agreement with a study of the sideways motion of Janus rods near a wall.[41] Moreover, the velocity of a single rod is stable during the measurement time, indicating no rotation around its long axis.

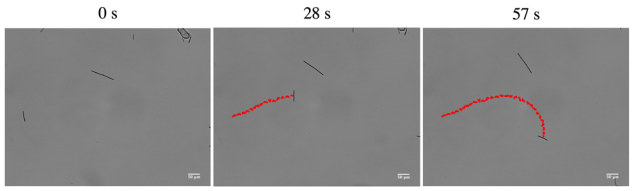

Fig. 2 Sideways propelled Pt/Au rod at the interface between an aqueous hydrogen peroxide solution (5 wt%) and *n*-decane, scale bar is 30 μm.

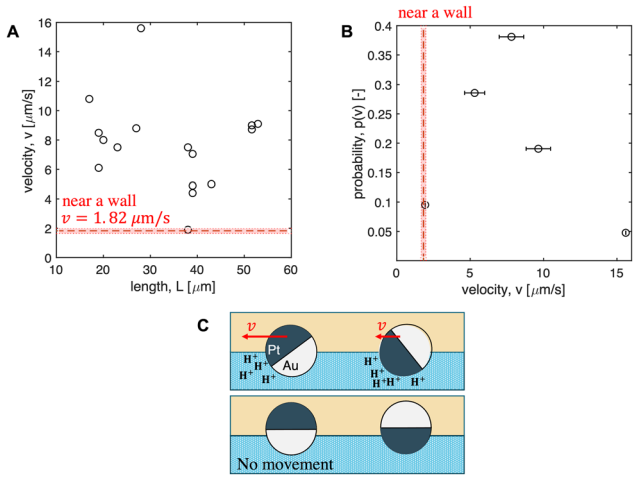

Fig. 3 (A) Velocities of Pt/Au sideways propelled rods at the interface between aqueous hydrogen peroxide (5 wt%) and *n*-decane *vs.* their lengths (over 21 rods). (B) The probabilities $p(v)$ of observing rods with velocities v. For clarity, velocities v that were in the range of ±10% from each other were combined together (resulting in 2, 8, 8, 4, and 1 rods per respective data point in the figure). Red dashed line: mean velocity of the rods near a wall; the red area represents the standard deviation. (C) Schematic of the proposed mechanism of the Pt/Au Janus rod propulsion, based on the studies of Dietrich *et al.*[30] The upper yellow phase is *n*-decane and the bottom blue phase is an aqueous solution of 5 wt% H_2O_2.

A significant difference in the Janus rod propulsion at the LLI when compared to their motion near a solid wall is the much wider distribution of the observed velocities. Most of the Pt/Au rods have a velocity in the range of 5–10 μm s^{-1}, with smaller fractions moving at velocities up to 16 μm s^{-1} and 2–5 μm s^{-1}. A similar tendency was also noticed for Pt/PS spherical particles at the LLI, which, however, have only two distinct sets of velocities, emerging from two prevailing particle orientations.[30] The term orientation here refers to the particular configuration of a Janus sphere or rod at the LLI, depending on how the boundary between the two metals (or the metal and the insulator) pierces the interface. It was shown that different orientations of a Janus particle give rise to concentration gradients of different strengths along the LLI, resulting in slower and faster sets of propelling particles.[30] For bimetallic Janus rods, we suggest a similar reason for the large distribution of velocities. The difference is, however, the mechanism of particle motion that dominates. There is strong evidence that bimetallic particle propulsion in hydrogen peroxide is induced by self-electrophoresis. According to this mechanism, Pt/Au particle motion is driven by a self-induced electric field due to electrochemical half-reactions occurring on Pt and Au:[50,51]

$$\text{Pt (anode): } H_2O_2 \rightarrow O_2 + 2H^+ + 2e^- \quad (2)$$

$$\text{Au (cathode): } H_2O_2 + 2H^+ + 2e^- \rightarrow 2H_2O \quad (3)$$

$$\text{Overall: } H_2O_2 \rightarrow O_2 + 2H_2O \quad (4)$$

Platinum and gold coatings act as an anode and cathode, respectively, producing an inhomogeneous distribution of protons along the particle surface. These protons are known to adsorb at air–water and oil–water interfaces,[52] which decreases their surface tension and modifies the ζ-potential. In particular, at pH ≈ 2–3 a number of liquid–fluid interfaces, including water/oil interfaces, have zero ζ-potential, which decreases with the increase of pH and for many water–oil systems equals $\zeta \sim -30$ mV at pH ≈ 4 (value for 5 wt% H_2O_2).[53] An inhomogeneous release of protons thus leads to a similar phenomenon as for self-diffusiophoretic Pt/PS particles, where the difference in propulsion velocities stems from the variation in electric field strength for different orientations of the rods as shown in Fig. 3C and not from concentration gradients. Note that in contrast to Pt/PS spheres,[30] only a fraction of the bimetallic Pt/Au rods propel. This is likely stemming from the larger number of bimetallic rods that have the contact line pinned at only one Janus side (as depicted in Fig. 3C, bottom image) compared to Pt/PS spheres. This configuration does not result in a self-induced electric field and is, therefore, immobile.

The self-propelled velocities of the particles at the LLI are found to be up to 8 times larger than their velocities near a solid wall, which can only be partially explained by the decreased viscous drag at the LLI compared to a solid boundary. Indeed, as pointed out by Wang *et al.*,[54] a particle's mobility near the LLI can be increased by reduced drag only by up to 3 times compared to that at a solid–liquid interface. We hypothesize that the enhancement in velocity is related to electrokinetic effects that is for example not present in catalytic systems where the motion does not stem from a self-induced electric field.[30] In particular, electroosmotic flow at the solid–liquid interface is known to decrease the velocity of self-electrophoretic particles by up to 25% compared to their bulk velocity.[55]

To calculate the thermodynamically favorable configuration of Janus rods at the LLI, defined by angles α and β in Fig. 4A, the

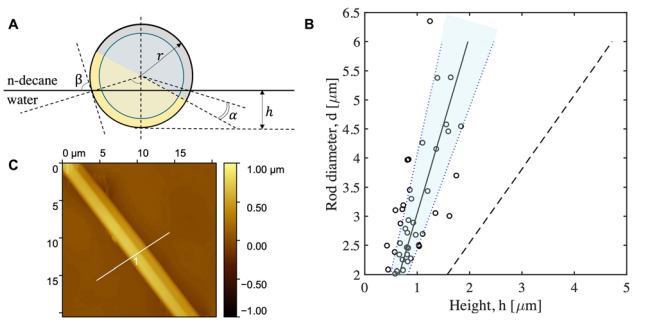

Fig. 4 (A) Schematic cross-section of a Janus cylinder at the interface between water and *n*-decane. α is the angle between the Janus boundary and the *n*-decane/water interface, while β is the contact angle of the rod. (B) Protrusion height h as a function of the diameter d of the cylinder. The theoretical equilibrium protrusion of a Janus rod is visualized by a solid line (hydrophobic Pt and Au surfaces) and a dashed line (hydrophilic Pt and Au surfaces after exposure to hydrogen peroxide). The experimentally measured protrusion height is shown by open circles, the blue area depicts 25% deviation from the theoretical protrusion height value. (C) Representative AFM image of the rod. The protrusion height is defined as the largest height measured along the white line.

wetting properties of rod's opposing surfaces need to be assessed. Macroscopic contact angles are measured for a water drop in *n*-decane on bare PS ($\Theta_{PS} = 144.5^\circ \pm 3.8^\circ$), on PS coated with Pt ($\Theta_{Pt} = 93^\circ \pm 2.4^\circ$) and PS coated with Au ($\Theta_{Au} = 101^\circ \pm 4.9^\circ$). Due to the small difference between Θ_{Pt} and Θ_{Au}, there is no preferential equilibrium orientation, and the angle α in Fig. 4A cannot be evaluated theoretically. However, the existence of a range of observed rod velocities suggests that, similarly to the study of Pt/PS spheres,[30] sideways propelled Janus rods are pinned at the LLI in different orientations due to their surface roughness.[56] For Pt/PS spheres, as discussed by Dietrich *et al.*, the particle orientations are truly metastable and different from the thermodynamically favorable one, while for Pt/Au rods no equilibrium configuration can be derived due to the fact that the contact angles for both metals are nearly identical.

The contact angles were also measured after placing the Pt/PS and Au/PS plates in H_2O_2 for 5 min. This allows us to determine and compare the equilibrium position of Janus rods both for the initial coating and after its exposure to hydrogen peroxide solution. Noble metals are known to considerably adsorb airborne hydrophobic contaminants, which results in larger contact angles, while the clean surfaces are usually more hydrophilic.[57] Hydrogen peroxide, being an oxidizer, is expected to clean the surface of the metals and thus decrease the measured contact angles. The resulting contact angles after exposure to H_2O_2 are in fact smaller and equal to $\Theta_{Pt,H_2O_2} = 58^\circ \pm 6.5^\circ$ and $\Theta_{Au,H_2O_2} = 65.4^\circ \pm 3.7^\circ$.

The angle β and thus the protrusion height h are then derived by finding the minimum of energy:

$$\Delta E = E - E_0, \tag{5}$$

where E and E_0 are the free energies of the system when the rod is trapped at the interface and of its initial state, respectively, which are defined as follows:

$$E = \gamma_{Pt,d}A_{Pt,d} + \gamma_{Pt,w}A_{Pt,w} + \gamma_{Au,d}A_{Au,d} + \gamma_{Au,w}A_{Au,w} + \gamma_{w,d}A_{w,d} - \gamma_{w,d}A_{int}, \tag{6}$$

$$E_0 = \pi rL(\gamma_{Pt,d} + \gamma_{Au,d}) + \gamma_{w,d}A_{w,d}, \tag{7}$$

where $\gamma_{Pt,d}$ and $\gamma_{Au,d}$ are the interfacial energies between Pt or Au and *n*-decane, $\gamma_{Pt,w}$ and $\gamma_{Au,w}$ are the interfacial energies between Pt or Au and water, $A_{Pt,d}$ and $A_{Au,d}$ are the rod surface areas coated with Pt and Au and exposed to *n*-decane, $A_{Pt,w}$ and $A_{Au,w}$ are the rod surface areas coated with Pt and Au and exposed to water, L is the rod length, $A_{w,d}$ is the water/*n*-decane interface area, A_{int} is the part of the water/*n*-decane interface area displaced by a Janus rod, r is the rod radius and $\gamma_{w,d}$ is the interfacial energy between water and *n*-decane.

The end of the Janus rod, where PS is exposed to both liquids, is not taken into account, since its area is relatively small compared to the overall surface of the Janus rod and does not have a significant influence on the obtained protrusion height. The theoretical protrusion height h for each rod diameter is visualized in Fig. 4B, both for the initial hydrophobic Pt and Au surfaces (solid line) and after their exposure to hydrogen peroxide (dashed line).

The real protrusion height of the Janus rods at the LLI was studied experimentally by AFM after trapping the particles in a PDMS layer. Fig. 4C shows an example of a Janus rod measured by AFM, for which the protrusion was calculated as the maximum height along the white line. As shown in Fig. 4B, the experimental data is close to the theoretical protrusion height of the neat metal surfaces, and differs from the theoretically calculated protrusion height after exposure to hydrogen peroxide. One of the reasons why the influence of H_2O_2 on the contact angle of a Janus rod is negligible could be the use of IPA:water as the spreading solution to distribute the particles at the water/*n*-decane interface, which can become trapped in metal surfaces heterogeneities.[58] Janus rods protrude more into the *n*-decane phase than into the aqueous phase. The large variability in the data is possibly the result of the multi-step gel trapping technique as well as the preparation procedure of the Janus rods.

To explain the large variation of velocities in Fig. 3A and B, we measured the orientation of Janus rods at the *n*-decane/water interface, defined by the angle α, using SEM EDX. Since the M lines in the EDX spectra of Pt and Au are not well-separated, an Ag coating, which has similar wetting properties as Pt,[59] was sputtered instead. Line scans along the diameter of the rods trapped in PDMS in the same configuration as at the *n*-decane/water interface revealed that most Janus rods have their boundary between the two metal coatings oriented horizontally along the *n*-decane/water interface. This configuration induces a homogeneous distribution of the reaction products at the oil/H_2O_2(aq.) interface and thus does not lead to propulsion, as, in fact, observed for the majority of the rods (Fig. 3). As shown in Fig. 5C, a smaller fraction of Janus rods has their boundary

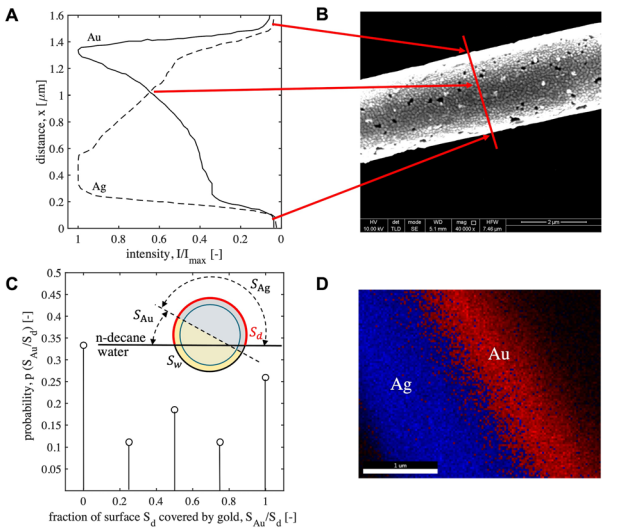

Fig. 5 (A) SEM EDX scan along the diameter of a Janus rod, solid line: gold; dashed line: silver. (B) SEM image of the Ag/Au Janus rod. (C) Probability distribution $p(S_{Au}/S_d)$ of the rods with varied fractions of gold S_{Au} exposed to the *n*-decane phase (over 27 rods). Inset: A schematic of a Janus rod at the *n*-decane/water interface showing the fractions of its surface S_w in water and S_d in *n*-decane as well as the surface coverage of the fraction S_d by gold S_{Au} and silver S_{Ag}. (D) SEM EDX elemental map of Janus rod; blue: silver (Ag), red: gold (Au).

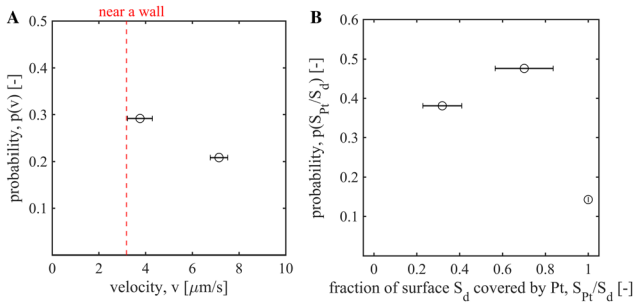

Fig. 6 (A) Probability $p(v)$ of observing Pt/PS rods with velocities v in the defined range (over 12 rods) at the interface between hydrogen peroxide dissolved in water (5 wt%) and *n*-decane. (B) Probability distribution $p(S_{Pt}/S_d)$ of the rods with varied fractions of platinum S_{Pt} exposed to the *n*-decane phase (over 21 rods).

between the two metal coatings piercing the interface at different angles. Fig. 5D shows an elemental map of a Janus fiber observed from the oil side. The majority of these configurations has equal Ag(Pt) and Au surface areas in both phases, while smaller fractions have one of the metals oriented more to the hydrogen peroxide phase. According to Dietrich *et al.*,[30] a larger velocity is induced by the configuration which produces steeper chemical gradients at the oil/water interface. Since the motion of Pt/Au relies on the gradient of protons produced on the platinum side, we expect that a Janus rod with less Pt in the hydrogen peroxide phase moves faster than those with a larger part of Pt in the hydrogen peroxide phase. Therefore, presumably, a rod with a smaller gold fraction in *n*-decane (and thus a smaller Pt fraction in water) induces a velocity larger than ~ 8 μm s^{-1}, while a rod with more gold coating in *n*-decane induces a velocity smaller than 8 μm s^{-1}. The intermediate configuration with equal parts of both metals in hydrogen peroxide solution is thus expected to result in intermediate velocities around 8 μm s^{-1}. As shown in Fig. 3, the probability of observing rods with this velocity is the largest across the velocity range, which is in good agreement with a larger probability of observing the intermediate configuration (Fig. 5C). Moreover, the propulsion experiments performed on Pt/PS rods indicate that the mechanism of propulsion is not influenced by the shape of the particle but solely by its orientation at the LLI. As shown in Fig. 6A, the velocities of Pt/PS rods are similar to Pt/PS spheres,[30] with two distinct sets of slower and faster particles. The presence of two preferred orientations of the rod, corresponding to a smaller and larger Pt part in the aqueous phase was also confirmed by SEM EDX analysis in Fig. 6B. Note that Pt/Au rod velocities at the LLI can be up to 8 times larger than their velocities near a wall, while the increase in the velocity of Pt/PS rods is only a factor two to three.

Finding a direct link between the orientation of a bimetallic Janus rod and its velocity, both measured *in situ*, is a promising direction to further understand its mechanism of propulsion, which is, however, outside of the scope of the current work.

4. Conclusions

We studied the motion of Pt/Au sideways propelled rods at the interface between an aqueous solution of hydrogen peroxide and *n*-decane. The protrusion of Janus rods at the LLI obtained by AFM is in good agreement with the theoretical predictions, indicating that the Janus rod protrudes more into the *n*-decane phase than into the aqueous one. The orientation of the metal coating with respect to the LLI was studied by SEM EDX and compared with the rod velocities in 5 wt% H_2O_2. Most of the rods were found to be oriented with the Janus boundary laying horizontally at the LLI, which agrees well with the observed ratio of motile:immotile rods. The motile fraction of rods is characterized by a wide distribution of velocities, which were correlated with the probabilities of observed orientations. The magnitude of observed velocities is larger than that of a sideways propelled rod near a solid wall and ranges from 2 μm s^{-1} up to 16 μm s^{-1}.

Our study, therefore, provides an experimental basis to modulate the propulsion of bimetallic anisotropic particles by trapping them at liquid–liquid interfaces.

Author contributions

Investigation: A. A., I. M., O. D., and W. M.; methodology: A. A., O. D., and W. M.; formal analysis: A. A., I. M., and O. D.; software: E. K. R.; supervision and conceptualization: N. R., J. F., and C. C. writing – original draft: A. A.; writing – review & editing: A. A., I. M., O. D., C. B., W. M., E. K. R., N. R., J. F., and C. C.

Conflicts of interest

There are no conflicts to declare.

Acknowledgements

The authors would like to acknowledge financial support from the FWO (Fonds voor Wetenschappelijk Onderzoek, Research Foundation Flanders, grant no. G077916N). C. Bartic and O. Deschaume acknowledge financial support from the Fonds voor Wetenschappelijk Onderzoek, Belgium (grant no. G0947.17N) and the Onderzoeksraad, KU Leuven, Belgium (grant no. C14/18/061).

Notes and references

1 C. Maggi, J. Simmchen, F. Saglimbeni, J. Katuri, M. Dipalo, F. De Angelis, S. Sanchez and R. Di Leonardo, *Small*, 2016, **12**, 446–451.
2 S. Balasubramanian, D. Kagan, C.-M. Jack Hu, S. Campuzano, M. J. Lobo-Castañon, N. Lim, D. Y. Kang, M. Zimmerman, L. Zhang and J. Wang, *Angew. Chem., Int. Ed.*, 2011, **50**, 4161–4164.
3 S. Sanchez, A. A. Solovev, S. Schulze and O. G. Schmidt, *Chem. Commun.*, 2011, **47**, 698–700.
4 S. Campuzano, J. Orozco, D. Kagan, M. Guix, W. Gao, S. Sattayasamitsathit, J. C. Claussen, A. Merkoçi and J. Wang, *Nano Lett.*, 2012, **12**, 396–401.

5 J. Orozco, S. Campuzano, D. Kagan, M. Zhou, W. Gao and J. Wang, *Anal. Chem.*, 2011, **83**, 7962–7969.
6 D. Kagan, P. Calvo-Marzal, S. Balasubramanian, S. Sattayasamitsathit, K. Manesh, G.-U. Flechsig and J. Wang, *J. Am. Chem. Soc.*, 2009, **131**, 12082–12083.
7 L. Sonntag, J. Simmchen and V. Magdanz, *Molecules*, 2019, **24**, 3410.
8 D. Patra, S. Sengupta, W. Duan, H. Zhang, R. Pavlick and A. Sen, *Nanoscale*, 2013, **5**, 1273–1283.
9 S. Ebbens and J. Howse, *Soft Matter*, 2010, **6**, 726–738.
10 W. Wang, W. Duan, S. Ahmed, T. E. Mallouk and A. Sen, *Nano Today*, 2013, **8**, 531–554.
11 A. Walther and A. H. Müller, *Soft Matter*, 2008, **4**, 663–668.
12 C. Maggi, F. Saglimbeni, M. Dipalo, F. D. Angelis and R. D. Leonardo, *Nat. Commun.*, 2015, **6**, 7855.
13 A. Domnguez, P. Malgaretti, M. N. Popescu and S. Dietrich, *Phys. Rev. Lett.*, 2016, **116**, 078301.
14 A. Arslanova, G. Natale, N. Reddy, C. Clasen and J. Fransaer, *Phys. Fluids*, 2020, **32**(12), 127109, DOI: **10.1063/5.0027309**.
15 S. Das, A. Garg, A. I. Campbell, J. Howse, A. Sen, D. Velegol, R. Golestanian and S. J. Ebbens, *Nat. Commun.*, 2015, **6**, 1–10.
16 W. Uspal, M. N. Popescu, S. Dietrich and M. Tasinkevych, *Soft Matter*, 2015, **11**, 434–438.
17 E. Yariv, *Phys. Rev. Fluids*, 2016, **1**, 032101.
18 P. Malgaretti, M. Popescu and S. Dietrich, *Soft Matter*, 2018, **14**, 1375–1388.
19 P. Malgaretti and J. Harting, *ChemNanoMat*, 2021, **7**, 1073–1081.
20 W. Fei, Y. Gu and K. J. Bishop, *Curr. Opin. Colloid Interface Sci.*, 2017, **32**, 57–68.
21 E. L. Correia, N. Brown and S. Razavi, *Nanomaterials*, 2021, **11**, 374.
22 B. J. Park, T. Brugarolas and D. Lee, *Soft Matter*, 2011, **7**, 6413–6417.
23 L. C. Bradley, W.-H. Chen, K. J. Stebe and D. Lee, *Curr. Opin. Colloid Interface Sci.*, 2017, **30**, 25–33.
24 B. J. Park and D. Lee, *ACS Nano*, 2012, **6**, 782–790.
25 A. Kumar, B. J. Park, F. Tu and D. Lee, *Soft Matter*, 2013, **9**, 6604–6617.
26 L. Isa, N. Samudrala and E. R. Dufresne, *Langmuir*, 2014, **30**, 5057–5063.
27 H.-M. Gao, Z.-Y. Lu, H. Liu, Z.-Y. Sun and L.-J. An, *J. Chem. Phys.*, 2014, **141**, 134907.
28 Z. Jalilvand, H. Haider, J. Cui and I. Kretzschmar, *Langmuir*, 2020, **36**, 6880–6887.
29 P. Sharan, W. Postek, T. Gemming, P. Garstecki and J. Simmchen, *Langmuir*, 2020, **37**, 204–210.
30 K. Dietrich, D. Renggli, M. Zanini, G. Volpe, I. Buttinoni and L. Isa, *New J. Phys.*, 2017, **19**, 065008.
31 N. Mano and A. Heller, *J. Am. Chem. Soc.*, 2005, **127**, 11574–11575.
32 X. Wang, M. In, C. Blanc, M. Nobili and A. Stocco, *Soft Matter*, 2015, **11**, 7376–7384.
33 G. Boniello, C. Blanc, D. Fedorenko, M. Medfai, N. B. Mbarek, M. In, M. Gross, A. Stocco and M. Nobili, *Nat. Mater.*, 2015, **14**, 908–911.
34 A. Stocco, B. Chollet, X. Wang, C. Blanc and M. Nobili, *J. Colloid Interface Sci.*, 2019, **542**, 363–369.
35 T. Peter, P. Malgaretti, N. Rivas, A. Scagliarini, J. Harting and S. Dietrich, *Soft Matter*, 2020, **16**, 3536–3547.
36 A. Dörr, S. Hardt, H. Masoud and H. A. Stone, *J. Fluid Mech.*, 2016, **790**, 607–618.
37 P. Malgaretti, M. Popescu and S. Dietrich, *Soft Matter*, 2016, **12**, 4007–4023.
38 P. Dhar, T. M. Fischer, Y. Wang, T. E. Mallouk, W. Paxton and A. Sen, *Nano Lett.*, 2006, **6**, 66–72.
39 A. Arslanova, V. R. Dugyala, E. K. Reichel, N. Reddy, J. Fransaer and C. Clasen, *Soft Matter*, 2021, **17**, 2369–2373, DOI: **10.1039/d1sm00042j**.
40 N. Reddy, L. Palangetic, L. Stappers, J. Buitenhuis, J. Fransaer and C. Clasen, *J. Mater. Chem. C*, 2013, **1**(23), 3646–3650, DOI: **10.1039/c3tc30176a**.
41 D. V. Rao, N. Reddy, J. Fransaer and C. Clasen, *J. Phys. D: Appl. Phys.*, 2019, **52**(1), 014002, DOI: **10.1088/1361-6463/aae6f6**.
42 H. R. Vutukuri, Z. Preisler, T. H. Besseling, A. Van Blaaderen, M. Dijkstra and W. T. Huck, *Soft Matter*, 2016, **12**, 9657–9665.
43 D. Li, Y. Wang and Y. Xia, *Nano Lett.*, 2003, **3**, 1167–1171.
44 B. Sundaray, V. Subramanian, T. Natarajan, R.-Z. Xiang, C.-C. Chang and W.-S. Fann, *Appl. Phys. Lett.*, 2004, **84**, 1222–1224.
45 V. N. Paunov and O. J. Cayre, *Adv. Mater.*, 2004, **16**, 788–791.
46 D. Nečas and P. Klapetek, *Open Phys.*, 2012, **10**, 181–188.
47 A. Goebel and K. Lunkenheimer, *Langmuir*, 1997, **13**, 369–372.
48 R. Bonhomme, J. Magnaudet, F. Duval and B. Piar, *J. Fluid Mech.*, 2012, **707**, 405–443.
49 G. M. Jang and N. I. Kim, *Fuel*, 2019, **240**, 1–9.
50 W. F. Paxton, P. T. Baker, T. R. Kline, Y. Wang, T. E. Mallouk and A. Sen, *J. Am. Chem. Soc.*, 2006, **128**, 14881–14888.
51 Y. Wang, R. Hernandez and D. Bartlett, *Langmuir*, 2006, **22**, 10451–10456.
52 S. I. Mamatkulov, C. Allolio, R. R. Netz and D. J. Bonthuis, *Angew. Chem., Int. Ed.*, 2017, **56**, 15846–15851.
53 N. Agmon, H. J. Bakker, R. K. Campen, R. H. Henchman, P. Pohl, S. Roke, M. Thämer and A. Hassanali, *Chem. Rev.*, 2016, **116**, 7642–7672.
54 G. Wang, R. Prabhakar, Y. Gao and E. M. Sevick, *J. Opt.*, 2011, **13**, 044009.
55 T.-Y. Chiang and D. Velegol, *Langmuir*, 2014, **30**, 2600–2607.
56 D. J. Adams, S. Adams, J. Melrose and A. C. Weaver, *Colloids Surf., A*, 2008, **317**, 360–365.
57 T. Smith, *J. Colloid Interface Sci.*, 1980, **75**, 51–55.
58 A. Maestro, L. J. Bonales, H. Ritacco, R. G. Rubio and F. Ortega, *Phys. Chem. Chem. Phys.*, 2010, **12**, 14115–14120.
59 F. Bartell and P. H. Cardwell, *J. Am. Chem. Soc.*, 1942, **64**, 494–497.

